ISSN 0915-633X

NATIONAL INSTITUTE FOR FUSION SCIENCE

Solution of Initial Value Problem of Gyro-Kinetic Equation

T. Yamagishi

(Received - Jan. 29, 1996)

NIFS-410 Mar. 1996

RESEARCH REPORT
NIFS Series

NAGOYA, JAPAN

Solution of Initial Value Problem of Gyro-Kinetic Equation

Tomejiro YAMAGISHI
Tokyo Metropolitan Institute of Technology

Abstract

Applying the Laplace transform technique, the initial value problem of gyro-kinetic equation is solved for the electrostatic ion temperature gradient instability situation in slab and toroidal systems. The transformed perturbed scalar potential, when evaluated on the real frequency axis, tends to small as the growth rate increases, and shows a singularity only at the marginal stability state. The time dependent solution for perturbed scalar potential is expressed in terms of the discrete mode and the continuum contribution. At the marginal stability state, the discrete eigenvalue attains the continuous eigenvalue spectrum. For the subcritical state the discrete eigenvalue moves into the next Riemann surface and tends to a damping mode, which has been numerically examined making use of the analytically continued dispersion relation. The time-dependent perturbed distribution is expressed in terms of the discrete mode, the velocity dependent beam mode, and the continuum contribution. Some characteristics of the discrete and continuum contribution are examined, and application to anomalous transport theory is suggested.

Keywords : toroidal plasma, dispersion relation, discrete eigenvalue, wave-particle resonance, continuum contribution, analytical continuation

§ 1. Introduction

Plasma instabilities have frequently been studied by solving the dispersion relation derived from the quasi-neutrality relation for gyro-kinetic solutions. Solving the dispersion relation is equivalent to calculating the discrete time eigenvalue ω_0 with some physical parameters. When the growth rate $\gamma=Im(\omega_0)$ is positive the plasma is said to be unstable, otherwise the plasma is stable, for certain perturbations. One of the most important characteristics of the Vlasov and gyro-kinetic transport equations is that they have both discrete and continuous eigenvalues[1][2][3][4]. Since the continuous eigenvalue induced by the wave particle resonance is independent of the discrete eigenvalue, i.e., instability, it has usually been neglected. Although the discrete mode may be more important than the continuum contribution, the existence of the discrete mode (instability) depends usually on some physical parameters. Since the continuum contribution always exists independently of the discrete mode, it may become important particularly when the discrete mode disappears.

When the discrete eigenvalue ω_0 is evaluated, from the saturation condition of the nonlinear growth rate $\gamma_{NL}=\gamma-k^2_\perp D_\perp=0$, the plasma diffusion coefficient is evaluated by $D_\perp=\gamma/k^2_\perp$. The plasma transport coefficient, on the other hand, is also evaluated by making use of the wave-particle resonance condition assuming perturbed scalar potentials exist. The latter approach is an evaluation of the continuum contribution. The above two methods look independent each other. However, when the complete solution for the scalar potential is derived, and expressed by the sum of the discrete mode and continuum contribution, these two approaches may be studied from an unified view point of gyro-kinetic eigenfunctions.

The purpose of the present paper is to solve the initial value problem of the gyro-kinetic equation and investigate the behavior of both discrete and continuum contributions of time dependent gyro-kinetic solution obtained by the Laplace transform technique for the electrostatic ion temperature gradient instability situation in slab and toroidal systems.

§ 2. Laplace Transformation of Gyro-Kinetic Equation

We start with the Vlasov equation for the perturbed distribution $\tilde{f}(\mathbf{r},\mathbf{v},t)$ in the toroidal coordinate system (r,θ,ϕ) in the electrostatic approximation

$$\frac{\partial \tilde{f}}{\partial t}+\boldsymbol{v}.\nabla\tilde{f}+\Omega\boldsymbol{v}\times\boldsymbol{b}\frac{\partial\tilde{f}}{\partial\boldsymbol{v}}=\frac{e}{M}\nabla\tilde{\phi}\frac{\partial f_0}{\partial\boldsymbol{v}}\ , \tag{1}$$

where the equilibrium distribution is given by $f_0=N(r)f_M(v)$ with $N(r)$ and f_M being, respectively, the unperturbed density and the Maxwellian distribution:

$$f_M(\mathbf{v})=\left(\frac{1}{\pi v_{th}^2}\right)^{\frac{3}{2}}\exp\left(-\left(\frac{v}{v_{th}}\right)^2\right)\ , \tag{2}$$

Ω=eB/Mc, v_{th} is the thermal velocity, $\tilde{\phi}$ is the perturbed scalar potential, and other notations are standard. Applying the Fourier expansion of the form

$$\tilde{f}(r,v,t) = \sum_k \tilde{f}(k,v,t) \exp(ik.r) \quad , \tag{3}$$

and bearing in mind the relations $v.\nabla = d/dt - \partial/\partial t$ and

$$\frac{\partial f_0}{\partial v} = -\frac{2}{v_{th}^2} v f_0 \frac{1}{\Omega} e_\theta \frac{\partial f_0}{\partial r} \quad ,$$

we have

$$(\frac{\partial}{\partial t} + v.\nabla + \Omega v \times b \frac{\partial}{\partial v})(\tilde{f} + \frac{e}{T}\tilde{\phi} f_0) = (\frac{\partial}{\partial t} + i\omega_T^*)\frac{e}{T}\tilde{\phi} f_0 \quad , \tag{4}$$

where $\omega^*_T=\omega^*(1+\eta(E-3/2))$ with $\omega^*=cTk_\theta/eBL_n$, $\eta=d\ln T/d\ln N$, $E=(v/v_{th})^2$ and $1/L_n=d\ln N/dr$.

We apply the Laplace transformation:

$$\hat{f}(k,v,\omega) = \int_0^\infty \tilde{f}(k,v,t)\exp(i\,\omega t)dt \quad ,$$

to the both sides of eq.(4), we obtain

$$(\omega - \omega_D - k_{\parallel} v_{\parallel})(\hat{f} + \frac{e}{T}\hat{\phi} f_0) = J_0^2(\alpha)(\omega - \omega_D)\frac{e}{T}\hat{\phi} f_0 + i\tilde{f}(k,v,0) \quad , \tag{5}$$

where $\omega_D=\mathbf{k}.\mathbf{v}_D$ with $\mathbf{v}_D=\mathbf{b}\times(v_\perp^2+v_\parallel^2)\nabla \ln B/\Omega$, being the curvature drift velocity. From eq.(5), we have the Laplace transformed gyro-kinetic solution in the form

$$\hat{f}(k,v,\omega) = -\left(1 - J_0^2(\alpha)\frac{\omega - \omega_T^*}{\omega - \omega_D - k_{\parallel} v_{\parallel}}\right)\frac{e}{T}\hat{\phi} f_0 + \frac{i\tilde{f}(k,v,0)}{\omega - \omega_D - k_{\parallel} v_{\parallel}} \quad . \tag{6}$$

For electrons, the transit frequency $k_{\parallel} v_{\parallel} \cong k_{\parallel} v_e$ may be much higher than ω and ω_{De}, the transformed solution may be approximated by

$$\hat{f}_e(k,v,\omega) = \frac{e}{T}\hat{\phi} f_{0e} \quad . \tag{7}$$

We apply eq.(6) for ions without subscript.

The perturbed density $\hat{n}$ is obtained by the velocity integration of $\hat{f}$:

$$\hat{n}(k,\omega) = -\left(1 - \int d^3v J_0^2(\alpha)\frac{\omega - \omega_T^*}{\omega - \omega_D - k_{\parallel} v_{\parallel}} f_M\right)\frac{e}{T}\hat{\phi} N + \int d^3v \frac{i\tilde{f}(k,v,0)}{\omega - \omega_D - k_{\parallel} v_{\parallel}} \quad . \tag{8}$$

The quasi-neutrality condition, $\hat{n}_e=\hat{n}$, then yields

$$\Lambda(k,\omega,\partial_r^2)\,\hat{\phi}(k,\omega,r) = i\,S(k,\omega) \quad , \tag{9}$$

where the no-dimensional quantity $e\hat{\phi}/T$ has been replaced by $\hat{\phi}$, and the dispersion function Λ and the source function S are defined as follows:

$$\Lambda(k,\omega,\partial_r^2) \equiv 1 + \frac{1}{\tau} - \int d^3v J_0^2(\alpha) \frac{\omega - \omega_T^*}{\omega - \omega_D - k_{\parallel} v_{\parallel}} f_M \quad , \tag{10}$$

$$S(k,\omega) \equiv \frac{1}{N} \int d^3v \frac{\tilde{f}(k,v,0)}{\omega - \omega_D - k_{\parallel} v_{\parallel}} \quad . \tag{11}$$

The argument in the Bessel function J_0 has been defined by $\alpha=(2b)^{1/2}v_{\perp}/v_{th,}$ with $b=(k_{\perp}v_{th})^2/2$ and $k_{\perp}^2=k_{\theta}^2-(\partial_r)^2$

Although the functional Λ involves the radial differential operator, for the sake of simplicity, here we neglect the radial variation of the eigenfunction $\hat{\phi}$, i.e., we assume the local mode approximation. In this case, Λ is a scalar function, and from eq.(9) we have

$$\hat{\phi}(k,\omega) = \frac{iS(k,\omega)}{\Lambda(k,\omega)} \, . \tag{12}$$

Introducing eqs.(10), (11) and (12) into eq.(8), we have the transformed density perturbation which is essentailly the same as the scalar potential:

$$\hat{n}(k,\omega) = \frac{iS(k,\omega)}{\Lambda(k,\omega)} \frac{N}{\tau} .$$

The time dependent solution can be obtained by the inverse Laplace transformation[5] of eq.(12):

$$\tilde{\phi}(k,t) = \frac{1}{2\pi} \int_{i\lambda-\infty}^{i\lambda+\infty} d\omega \exp(-i\omega t) \frac{iS(k,\omega)}{\Lambda(k,\omega)} \quad , \tag{13}$$

where λ is a maximum positive constant for which $\tilde{\phi}$ can exists.

§ 3. Inverse Laplace Transformation for Transit Resonance Case

To perform the Laplace inversion, we have to know the detail analytical property of the integrand in eq.(13). The integrand usually has a pole at $\omega=\omega_0$ given by the dispersion relation

$$\Lambda(k,\omega) = 0 \quad . \tag{14}$$

The solution ω_0 of eq. (14), corresponds to the discrete eigenvalue. The real part, $Re\omega_0$, is the oscillation frequency and the imaginary part, $Im\omega_0$, gives the growth rate of particular instability. The function S and Λ involve the singular integral at the wave particle resonance condition

$$\omega=\omega_D(v)+k_{\parallel} v_{\parallel} \qquad \text{for all } v \tag{15}$$

which occupies a part of the real axis which forms the continuum in the complex ω-plane. The integrand is discontinuous across the continuum, i.e., the continuum is the boundary of the analytical region of the integrand in the complex ω-plane. The set of frequencies (the part of the real axis) given by eq.(15) corresponds to the continuous eigenvalue.

Here we examine the analytical property of the dispersion function in some details. If we employ the normalized variables $x=v_{\perp}/v_{th}$ and $y=v_{\parallel}/v_{th}$, eq.(10) can be written in the double integral form:

$$\Lambda(\omega) = 1 + \frac{1}{\tau} - \frac{2}{\sqrt{\pi}}\int_0^\infty dx x e^{-x^2} J_0^2(\sqrt{2b}x) I(x,\omega) , \tag{16}$$

where

$$I(x,\omega) = \int_{-\infty}^{\infty} dy e^{-y^2} \frac{\omega - \omega_T^*(1+\eta(x^2+y^2-3/2))}{\omega - \omega_D(x^2/2+y^2) - \omega_t y} . \tag{17}$$

When the curvature drift effect is neglected, $\omega_D \to 0$, the resonance condition is simplified to the purely transit resonance, $\omega=\omega_t$ y. In this case the continuum occupies the whole real axis in the complex ω-plane. The dispersion function $\Lambda(\omega)$ becomes discontinuous across the real axis, and eq.(16) reduces to the usual form:

$$\Lambda(\omega) = 1 + \frac{1}{\tau} + \zeta\left[\left(1 - \frac{\omega^*}{\omega}\right)\Gamma_0 + \frac{\omega^*}{\omega}\eta\left\{\left(\frac{1}{2}\Gamma_0 - b(\Gamma_1 - \Gamma_0)\right)Z_0 - \Gamma_0 Z_2\right\}\right] , \tag{18}$$

where Γ_j=exp(-b) I_j , I_j is the modified Bessel function and Z_j is the moment of the plasma dispersion function[6]:

$$Z_j(\zeta) = \frac{1}{\sqrt{\pi}}\int_{-\infty}^{\infty} \frac{du e^{-u^2} u^j}{u - \zeta} . \tag{19}$$

The Laplace inversion in eq.(13) may be carried out by making a closed rectangular contour as shown in Fig. 1, and shifting the vertical paths in the left and right sides to the left and right infinity, respectively. Since the integral along the vertical paths tends to zero as they move to infinity, the inversion path can be replaced by the residue at the pole ω_0 and the integral along the real axis (continuum). If the pole given by eq.(14) is in the upper half ω-plane ($\mathrm{Im}\omega_0 > 0$), the inverse Laplace integral (13) can be expressed in the form

$$\tilde{\phi}(k,t) = \frac{S(k,\omega_0)}{\Lambda'(k,\omega_0)} \exp(-i\omega_0 t) + \frac{i}{2\pi}\int_{-\infty}^{\infty} d\omega \exp(-i\omega t) \frac{S^+(k,\omega)}{\Lambda^+(k,\omega)} , \tag{20}$$

where Λ' means the derivative with respect to ω, $\Lambda^{\pm}$ has been defined by

$$\Lambda^{\pm}(k,\omega) = \lim_{\varepsilon \to 0} \Lambda(k, \omega \pm i\varepsilon), \tag{21}$$

and $S^{\pm}$ are defined in the same manner. The first term in eq.(20) is the discrete mode, and the second integral corresponds to the continuum contribution.

When the pole ω_0 is in the lower half plane, the pole contribution may be evaluated by analytical continuation of Λ^+ into the lower half plane and pick up the residue at the pole ω_0 as shown by the dotted contour in Fig.1. In this case, the pole ω_0 itself is evaluated as the solution of the analytically continued dispersion relation $\Lambda^+(\omega_0)=0$, and the negative growth rate $\gamma=\mathrm{Im}\omega_0$ gives the Landau damping. The Laplace inversion can be expressed in the form

$$\tilde{\phi}(k,t) = \frac{S(k,\omega_0)}{\Lambda^{+\prime}(k,\omega_0)} \exp(-i\omega_0 t) + \frac{i}{2\pi}\int_{-\infty}^{\infty} d\omega \exp(-i\omega t) P \frac{S^+(k,\omega)}{\Lambda^+(k,\omega)} ,$$

where P means Chauchy's principal value integral.

By the same way, introducing eq.(12) into eq.(6) neglecting ω_D, the time-dependent distribution f can be obtained by the inverse Laplace transformation of eq.(6). In this case, additional singularity apprears from the resonance denominator (ω-$k_{\parallel} v_{\parallel}$) in eq.(6). Applying the Plemeli formula for the resonance denominator,

$$\frac{1}{x \pm i0} = P\frac{1}{x} \mp i\pi\,\delta(x), \tag{22}$$

and taking the same path integral as shown in Fig.1, the inverse Laplace transformation of eq.(6) for $\omega_D = 0$, yields the time-dependent solution:

$$\tilde{f}(k,v,t) = \left(1 - J_0^2 \frac{\omega_0 - \omega_T^*}{\omega_0 - k_{\parallel} v_{\parallel}}\right) \frac{iS(\omega_0)}{\Lambda'(\omega_0)} f_0 e^{-i\omega_0 t} - \frac{1}{2}\left\{ J_0^2 (k_{\parallel} v_{\parallel} - \omega_T^*) \frac{iS(k_{\parallel} v_{\parallel})}{\Lambda'(k_{\parallel} v_{\parallel})} f_0 + \tilde{f}(k,v,0) \right\} e^{-ik_{\parallel} v_{\parallel} t}$$

$$+ \frac{i}{2\pi} \int_{-\infty}^{\infty} d\omega e^{-i\omega t} \left\{ \left(1 - J_0^2 P \frac{\omega - \omega_T^*}{\omega - k_{\parallel} v_{\parallel}}\right) \frac{iS^+}{\Lambda^+} f_0 - P \frac{\tilde{f}(k,v,0)}{\omega - k_{\parallel} v_{\parallel}} \right\} . \tag{23}$$

The first term in eq.(23) is the discrete mode, the second velocity-dependent term is the beam mode comes from the singularity in the continuum contribution, and the third term represents the continuum contribution. The notation P in eq.(23) means the principal value intgral. If we integrate the both sides of eq.(23) over velocity v, we have the time dependent peturbed density $\tilde{n}(k,t)$ which coinsides with the one derived by inverse Laplace transformation of $\hat{n}(k,\omega)$.

§ 4. Case of Ion Temperature Gradient Instability

We now consider the initial value problem of the ion temperature gradient mode in a toroidal system, and return to eq.(16). If the curvature drift frequency ω_D is included, eq(17) can be written in the form

$$I(x,\omega) = -\frac{2}{\bar{\omega}_D \sqrt{\pi}} \int_{-\infty}^{\infty} \frac{dy e^{-y^2}}{(y - y_+)(y - y_-)} , \tag{24}$$

where

$$y_{\pm} = \frac{1}{2}\left\{ -\bar{\omega}_t \pm \left(\bar{\omega}_t^2 + 4(\bar{\omega} + \frac{x^2}{2}) \right)^{\frac{1}{2}} \right\} , \tag{25}$$

and $\bar{\omega}$ and $\bar{\omega}_t$ mean the normalization by ω_D . The integral given by eq.(20) can be expressed in terms of the plasma dispersion function Z_0. Introducing thus obtained into eq.(16), we have

$$\Lambda(\omega) = 1 + \frac{1}{\tau} + \int_0^{\infty} dx x e^{-x^2} J_0^2(\sqrt{2b}x) \frac{Z_0(y_+) - Z_0(y_-)}{\bar{\omega}_D \left\{ \bar{\omega}_t^2 + 4(\bar{\omega} + x^2/2) \right\}^{1/2}} . \tag{26}$$

The square root function $\{\omega_t^2 + 4(\omega + x^2/2)\}^{1/2}$ in eqs.(25) and (26) has the branch points at

$\omega=-x^2/2-(\omega_t/2)^2$ and $\omega=-\infty$ in the complex $\bar{\omega}$-plane. This square root function and therefore the dispersion function $\Lambda(\bar{\omega})$ is discontinuous across the branch cut which extends between these branch points on the real axis in the complex $\bar{\omega}$-plane. Notice that as compared with the case of $\omega_D=0$, the continuum(the branch cut) has been changed from the whole real axis to the part of the real axis: $-\infty<\bar{\omega}<-\bar{\omega}_t^2/4\omega_D$, i.e., the function $\Lambda(\bar{\omega})$ becomes continuous across the real axis in the region $\bar{\omega}>-\bar{\omega}_t^2/4\omega_D$. When $\omega_D \to 0$, the continuum is reduced to the whole real axis as shown the first transit resonance case.

When the transit frequency is neglected ($\omega_t=0$), eq.(25) reduces to $y_{\pm}=\pm(\omega+x^2/2)^{1/2}$. Applying the relation $Z_0(-\zeta)=-Z_0(\zeta)$ to eq.(26), we have

$$\Lambda(\omega) = 1+\frac{1}{\tau}+\int_0^{\infty} dx x e^{-x^2} J_0^2(\sqrt{2b}x)\frac{Z_0(y_+)}{\bar{\omega}_D(\bar{\omega}+x^2/2)^{1/2}} \quad . \tag{27}$$

In this case, the branch cut (continuum) for the square root function becomes the negative real axis:$-\infty<\omega<0$. In this case too, analytical evaluation of eq.(27) may be difficult due to the square root and the Bessel function. Equation (27) may be useful for numerical evaluation.

The major complexity in eqs. (26) and (27) comes from the Bessel function and the expression of the curvature drift frequency ω_D by two variables x and y. For the sake of simplicity, we here assume that the ion Larmor radius is negligibly small, $\alpha \to 0$, the ion transit frequency is also negligibly low, $\omega_t \to 0$, and the curvature drift frequency is proportional to the normalized energy E: $\omega_D=\hat{\omega}_D E$. In this case, the dispersion function Λ is expressed by the single integral:

$$\Lambda(k,\omega) = 1+\frac{1}{\tau}-\frac{2}{\sqrt{\pi}}\int_0^{\infty}\frac{\omega-\omega^*(1+\eta(E-3/2))}{\omega-\hat{\omega}_D E}\sqrt{E}\exp(-E)dE \quad , \tag{28}$$

which can be written in term of the usual plasma dispersion function Z in the form

$$\Lambda(k,\omega) = 1+\frac{1}{\tau}-\bar{\omega}^*\eta-2\left\{\bar{\omega}^*(1-\frac{3}{2}\eta)-\bar{\omega}(1-\bar{\omega}^*\eta)\right\}\left\{1+\sqrt{\bar{\omega}}Z(\sqrt{\bar{\omega}})\right\} \quad , \tag{29}$$

where the bar over frequencies mean the normalization by ω_D. The plasma dispersion function is numerically evaluated by the integral formula for $\mathrm{Im}\zeta>0$,

$$Z(\zeta) = 2i\exp(-\zeta^2)\int_{-\infty}^{i\zeta}\exp(-u^2)du \quad , \tag{30}$$

where the complex integral in eq.(30) is understood as the path integral from $-\infty$ to $-\mathrm{Im}\zeta$ along the real axis plus the path integral from $-\mathrm{Im}\zeta$ on the real axis to $i\zeta$. Since the integrand in eq.(30) is analytic, by making use of the analytical continuation, the integral path can off course be deformed to any other convenient form. For $\mathrm{Im}\zeta \to 0$, i.e., ζ is on the real axis, eq(20) reduces to the usual formula

$$Z^+(x) = \exp(-x^2)\left(i\sqrt{\pi}-2\int_0^x \exp(u^2)du\right) \quad . \tag{31}$$

The imaginary part of eq.(31), which corresponds to the δ-function term in the Plemeji formula (22), is explicitly separated from the real integral part.

We assume a simple approximation: $\hat{\omega}_D=2\varepsilon_n\omega^*$ where $\varepsilon_n=L_n/R$ and R is the major radius. In this case, the discrete eigenvalue ω_0 given by $\Lambda(k,\omega_0)=0$ depends on two parameters η and ε_n. For fixed η, the discrete eigenvalue ω_0 tends to negative real axis as ε_n increases[7].

The negative real axis is the continuous eigenvalue given by the condition (15) for $k_\parallel v_\parallel =0$. Although the Z-function is discontinuous on the whole real axis, in our problem, the argument is always the square root type as seen in eq.(26). The square root function $\omega^{1/2}$ has the branch cut on the negative real axis. The function $Z(\omega^{1/2})$ is, therefore, discontinuous across the branch cut, and continuous on the positive real axis. This branch cut corresponds to the continuum given by the resonance condition $\omega=\omega_D(v)$.

The limiting value of the dispersion function Λ^+ on the negative real axis can be analytically derived by introducing eq.(31) into eq.(29). The real and imaginary parts of the dispersion function Λ^+ can be written

$$\mathrm{Re}\,\Lambda^+ \equiv \Lambda_p = 1+\frac{1}{\tau}-\overline{\omega^*}\eta-2\left\{\overline{\omega^*}\left(1-\frac{3}{2}\right)+\bar{\omega}(1-\overline{\omega^*}\eta)\right\}\left(1+i\sqrt{\bar{\omega}}\,\mathrm{Re}\,Z^+\right) \quad , \tag{32}$$

$$\mathrm{Im}\,\Lambda^+ \equiv \pi j_i = -2\left\{\overline{\omega^*}\left(1-\frac{3}{2}\right)+\bar{\omega}(1-\overline{\omega^*}\eta)\right\}\sqrt{\pi}\exp(-\bar{\omega}) \quad . \tag{33}$$

The marginal stability condition, $\mathrm{Im}\omega=0$, can be derived from $\Lambda^+(\omega)=0$ for real ω. Applying eqs.(32) and (33), we have the critical condition for a fixed ε_n:

$$\eta_c = 2\left(1+\frac{1}{\tau}\right)\varepsilon_n \quad . \tag{34}$$

The numerical factor 2 in eq. (24) is larger than 4/3 in the same formula derived by Guo et al[8], which may be due to the difference of the numerical factor in the drift frequency : $\hat{\omega}_D=2\varepsilon_n\omega^*$. When η is fixed, the critical condition for ε_n becomes $\varepsilon_c=\tau\eta/2(1+\tau)$. Above the critical value, $\varepsilon_n > \varepsilon_c$, the instability is suppressed. The normalized frequency at the critical condition is obtained in the form

$$\frac{\omega}{\omega^*} = 1-3(1+\tau)\varepsilon_n \quad . \tag{35}$$

Situations of the discrete eigenvalue ω_0 and the branch cut (continuum) for the ITG mode in the complex ω-plane is shwon in Fig.2. The branch cut is the boundary of the analytic region of Λ. We can examine the existence of the zero point ω_0 of Λ by plotting the limitting function Λ^+ and Λ^- in the complex Λ-plane. As seen in Fig.3, the complex function Λ^+ and Λ^- form a closed contour in the complex Λ-plane. The contours of Λ^+ and Λ^- in Fig.3 also indicate that how much the limiting dispersion function Λ^+ and Λ^- are discontinuous across the branch cut. When the closed contour encircles the origin (the case of $\varepsilon_n=0.4(\bar{\omega}_D=1.25)$) the zero point ω_0 exists, while if the closed contour does not encircle the origin (the case of $\varepsilon_n=0.6(\bar{\omega}_D=0.833)$) Λ has no zero point in the complex ω-plane.

We now investigate how the discrete eigenvalue moves after it attains the continuum for $\varepsilon_n > \varepsilon_c$. The discrete eigenvalue may move into the lower half ω-plane (next Riemann surface) across the real axis as in the case of the slowing down continuum[9]. Although the limiting dispersion function Λ^+ is defined only on the negative real axis, we apply the same dispersion function by analytically continuing into the lower complex ω-plane, and calculate the solution ω_0 of $\Lambda^+(\omega_0)=0$ for $\varepsilon_n > \varepsilon_c$. As mentioned in the above, Λ is a function of $\omega^{1/2}$ which is also discontinuous across the branch cut. To make the analytical continuation to the lower ω-plane, both Λ and $\omega^{1/2}$ should be continued analytically across the branch cut. Since $\omega^{1/2}$ can be continuous by multiplying $\exp(\pi i)= -1$, the analytical continuation of the dispersion function can be made by using Λ^+ with the argument $-\omega^{1/2}$ when we cross the branch cut from the upper to lower planes. We numerically calculated the analytically continued dispersion relation, and found that the solution ω_0 actually moves into the lower ω-plane (next Riemann surface) as shown in Fig. 4. This means that the discrete mode becomes a damping mode ($\mathrm{Im}\omega_0<0$) for $\varepsilon_n>\varepsilon_c$.

Let us evaluate the time dependent solution by the inverse Laplace transformation (13). Since the integrand in eq.(13) is analytic in the complex ω-plane except the branch cut and pole, the inversion path in the present case may be connected to form a closed path as shown in Fig. 2. The integral along this closed contour is zero. Since the path integral on the large half circle vanishes as the radius tends to infinity, the inversion path can be replaced the residue at the pole $\omega=\omega_0$ and the integral around the branch cut (continuum). The time dependent solution can be written in the form

$$\tilde{\phi}(k,t) = \frac{S(k,\omega_0)}{\Lambda'(k,\omega_0)}\exp(-i\omega_0 t) - \frac{i}{2\pi}\int_{-\infty}^{0} d\omega \exp(-i\omega t)\left\{\frac{S^+(k,\omega)}{\Lambda^+(k,\omega)} - \frac{S^-(k,\omega)}{\Lambda^-(k,\omega)}\right\} \quad . \qquad (36)$$

The absolute values of scalar potential $|\phi|=|S^+/\Lambda^+|$ on the negative real axis behaves as shown in Fig.5. The potential shows singularity as the discrete mode tends to the continuum (the case of $\omega_D=0.833$) or the ITG growth rate tends to zero. For unstable states with large growth rate, the potential becomes small in the present linear theory. This means that strong instabilities may not be found from the scalar potential spectrum as long as it is evaluated on the real frequency axis. The strong singularity may happen only when the instability is close to the marginal state. This situation may be applicable to any other instabilities. This may be a reason why it is usually difficult to find clear correlation between the linear instability and observed frequency power spectrum of scalar potentials.

When the discrete eigenvalue ω_0 tends to the continuum, the first term in eq.(36) disappears, and the solution is expressed by the second continuum contribution alone. In this case the discrete eigenvalue ω_0 is embedded in the continuum, and the first term in the integrand in eq.(36) has an isolated singularity due to $\Lambda^+(\omega_0)=0$. At the same time the second term also becomes singular because $\Lambda^-(\omega_0)=0$. In this case, the integral around the continuum may be deformed to encircle the pole as shown in Fig.6. Because the path integral along the half circle can be replaced by the

half residue, the second integral in eq.(26) can be written in the form

$$\tilde{\phi}(k,t) = \frac{1}{2}\left(\frac{S^+}{\Lambda^{+\prime}} - \frac{S^-}{\Lambda^{-\prime}}\right)_{\omega=\omega_0} \exp(-i\omega_0 t) - \frac{i}{2\pi}\int_{-\infty}^{0} d\omega \exp(-i\omega t)\left\{\frac{S^+(k,\omega)}{\Lambda^+(k,\omega)} - \frac{S^-(k,\omega)}{\Lambda^-(k,\omega)}\right\}, \quad (37)$$

where the prime means the differentiation with respect to ω and integral in the second term in eq. (37) means the integral except the singularity at $\bar{\omega}=\omega_0$. As seen in eq.(37), even when the discrete eigenvalue is embedded in the continuum, the discrete mode can be separated from the continuum contribution with different coefficient. The discrete mode in this case is an oscillating stationary mode.

The time dependent solution for Vlasov equation can be obtained by the same method. Since the transformed solution $\hat{f}$ has the same singularity as $\hat{\phi}$ in the complex $\bar{\omega}$-plane, $\tilde{f}$ can be derived by introducing eq.(12) into eq.(6), and then performing the inverse Laplace transformation in the form:

$$\tilde{f}(k,v,t) = \left(1 - J_0^2\frac{\omega-\omega_T^*}{\omega-\omega_D}\right)\frac{S(k,\omega_0)}{\Lambda'(k,\omega_0)}e^{-i\omega_0 t} - J_0^2(\alpha)(\omega_D-\omega_T^*)\frac{S^+(k,\omega_D)}{\Lambda^+(k,\omega_D)}e^{-i\omega_D t}$$

$$+\frac{i}{2\pi}\int_{-\infty}^{0} d\omega\left(1 - J_0^2 P\frac{\omega-\omega_T^*}{\omega-\omega_D}\right)e^{-i\omega t}\left\{\frac{S^+}{\Lambda^+} - \frac{S^-}{\Lambda^-}\right\} - \frac{1}{2\pi}\tilde{f}(k,v,0)\int_{-\infty}^{0}\frac{d\omega e^{-i\omega t}}{\omega - \omega_D E}, \quad (38)$$

where the first term represents the discrete ITG mode, the second term is the velocity dependent beam mode which comes from the δ-function term (the compliment of the principal value integral) in the continuum integral, the third term is the continuum integral around the branch cut, and the fourth term represent the source.

§ 5. Summary

The time dependent solution for the perturbed scalar potential and gyro-kinetic equation have been derived making use of the Laplace transform technique for the cases of ion temperature gradient instability in the slab and toroidal system. In the slab geometry case of transit resonance $\omega=k_{\parallel}v_{\parallel}$, the continuum consists of whole real axis across which the dispersion function becomes discontinous as in usual case. While in the toroidal system, the drift resonance condition $\omega=\omega_D(v)+k_{\parallel}v_{\parallel}$ limits the continuum to a part of the real axis. Across the complimentary part of the real axis, the dispersion function becomes continous, and the analytical continuation into the lower half complex plane can be made through the complimentary part of the real axis.

The time-dependent solution for the perturbed scalar potential has been expressed by the sum of the discrete mode and the continuum contribution (Van Kampen mode). The solution for the perturbed distribution is expressed by the similar but more complicated form, i.e., the continuum

contribution is separated into the velocity dependent beam mode and the usual integral along the branch cut. The variation of the discrete eigenvalue ω_o has numerically been examined for a simple model of the dispersion function. When ε_n increases, ω_o attains the continuum (negative real axis) at the critical condition $\varepsilon_n=\varepsilon_c$. For the subcritical state $\varepsilon_n>\varepsilon_c$, the eigenvalue $\omega_o$moves into the next Riemann surface, and changes to the damping mode, which has been confirmed by numerically evaluating the analytically continued dispersion function across the branch cut.

Behavior of the frequency dependence of transformed scalar potential $\hat{\phi}(k,\omega)$ given by eq.(12) has also be examined for various values of ε_n. The frequency spectrum of amplitute $|\hat{\phi}(k,\omega)|$ becomes lower level as the growth rate increases. The spectrum evaluated on the real frequency axis shows singularity only at the marginal stability condition in the linear theory. This may be the reason why the linear instability is difficult to observe from the real frequency spectrum of transformed scalar potential.

To apply the present result to anomalous plasma transport theory, the autocorrelation $<\tilde{\phi},\tilde{\phi}>$ has to be evaluated. Since the discrete and continuum modes can be interpreted as the coherent $\tilde{\phi}_c$ and incoherent $\tilde{\phi}_{ic}$ modes, respectively, and they are orthogonal with respect to the ensamble average: $<\tilde{\phi}_c,\tilde{\phi}_{ic}>=0$, the transport coeffiients may also be expressed by the sum of the discrete and continuum contributions, $<\tilde{\phi}_c,\tilde{\phi}_c>$ and $<\tilde{\phi}_{ic},\tilde{\phi}_{ic}>$, respectively. In this way we may constract an unified theory to anomalous transports. Detail of the application will be published elsewhere.

Acknowledgement

This study is a joint research effort with the National Institute for Fusion Science.

References

[1]K.M.Case, Annals of Physics,**7**(1959)349.

[2]K.M.Case and P.F.Zweifel, *Linear Transport Theory*,Addison-Wesley,New York,1967.

[3]T.Yamagishi, Transport Theory and Statistical Physics,**3**(1973)107.

[4]N.G.Van Kampen and B.V.Felderhof,*Theoretical Methods in Plasma Physics*(translated into Japanese by M.Nishida), Kinokuniya, Tokyo, 1973.

[5]T.Yamagishi, J.Phys.D:Appl.Phys.,**7**(1974)510.

[6]T.Yamagishi, Plasma Physics and Cont. Fusion, **28**(1986)453.

[7]T.Yamagishi, *Cross Field Energy Flux due to Ion Temperature Gradient Mode*, American Institute of Physics, Conference Proceeding,No.284(1993)340.

[8]S.C.Guo and R.Romanelli, Phys. Fluids B**5**(1993)520.

[9]T.Yamsgishi, Nucl.Fusion, **31**(1991)1540.

Figures Captions

Fig.1: Laplace inversion contour for the transit resonance case in a slab. The small circle around the pole ω_0 gives the residue.The dotted circle in the lower plane indicates the case of analytical continuation for the damping mode.

Fig.2: Deformation of the Laplace inversion contour for the ITG mode in the complex ω-plane.

Fig.3: Variations of the limiting dispersion functions Λ^+ and Λ^- around the branch cut for different values of ε_n.

Fig.4: Trajectories of discrete eigenvalue ω_0 for η-mode for various values of ε_n. Dotted curves represent analytically continued ω_0 to the next Riemann surface.

Fig.5: Variations of scalar potential $\phi=|S^+/\Lambda^+|$ along the branch cut.

Fig.6: Deformation of the integral path around the continuum when the pole ω_0 is embedded in the continuum.

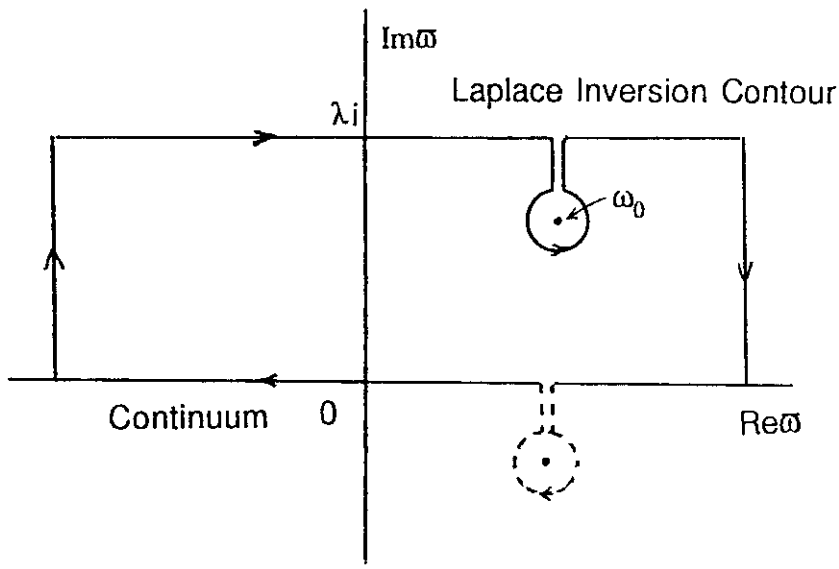
Imϖ
Laplace Inversion Contour
λi
ω_0
Continuum
0
Reϖ

Fig.1

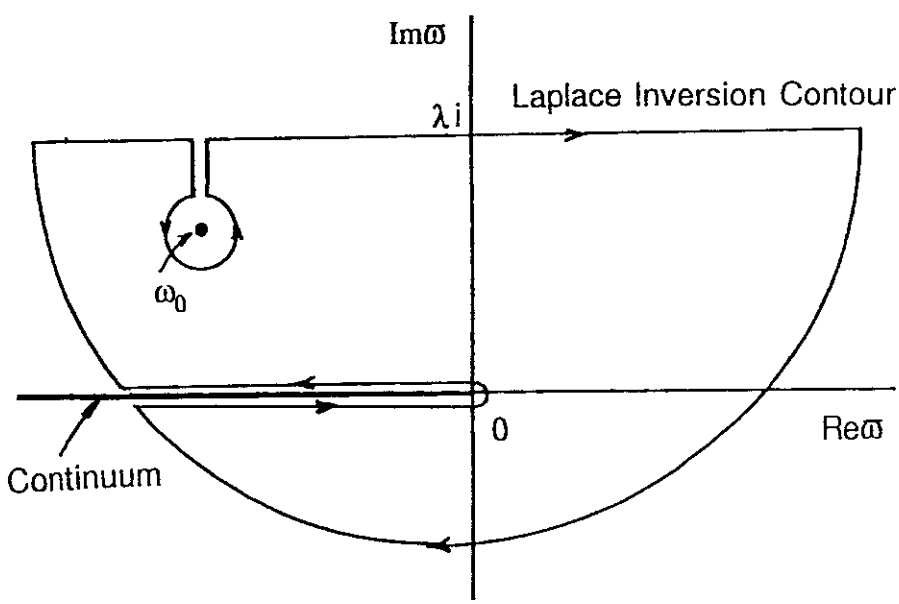
Imϖ
Laplace Inversion Contour
λi
ω_0
0
Reϖ
Continuum

Fig. 2

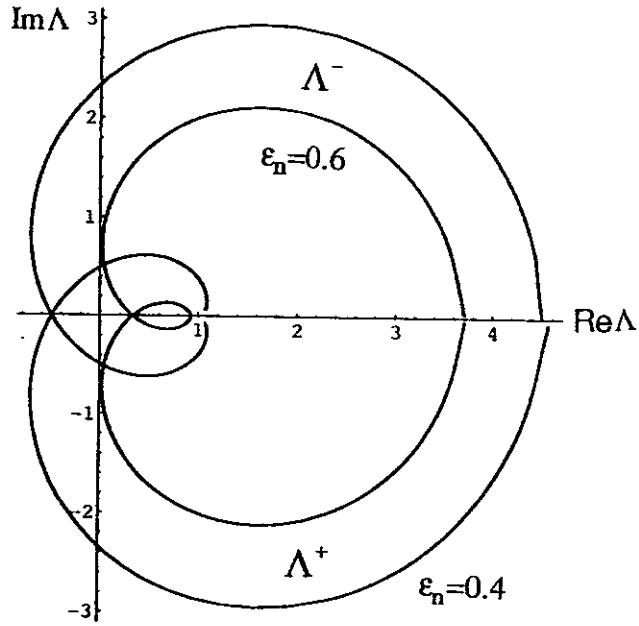
ImΛ
ReΛ
Λ⁻
Λ⁺
εn=0.6
εn=0.4

Fig.3

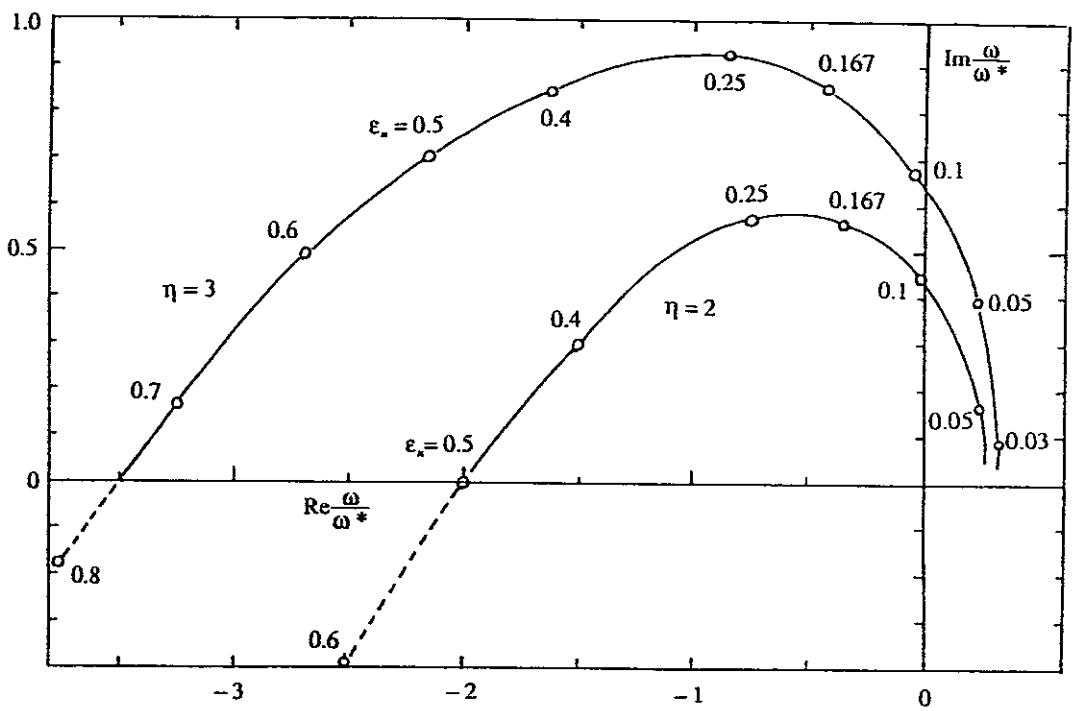
Im ω/ω*
Re ω/ω*
η = 3
η = 2
εn = 0.5
εn = 0.5
0.167
0.25
0.4
0.6
0.7
0.8
0.1
0.05
0.03
0.167
0.25
0.4
0.6
0.1
0.05

Fig.4

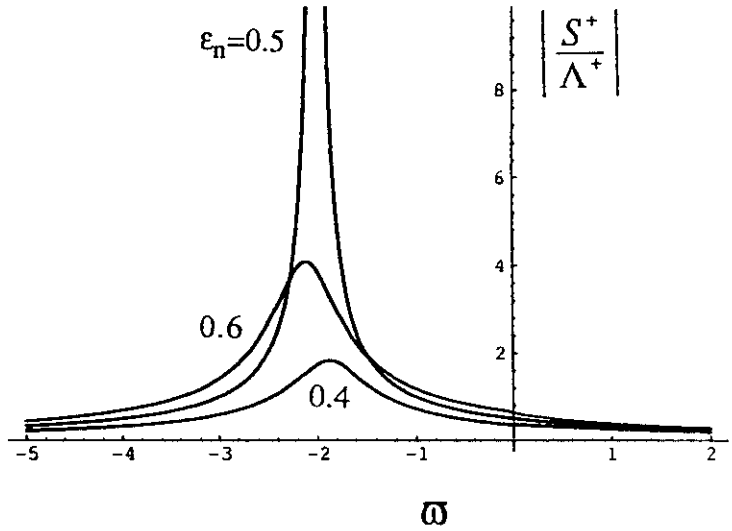
ε_n=0.5
0.6
0.4
$\left|\frac{S^+}{\Lambda^+}\right|$
8
6
4
2
-5
-4
-3
-2
-1
1
2
ϖ

Fig.5

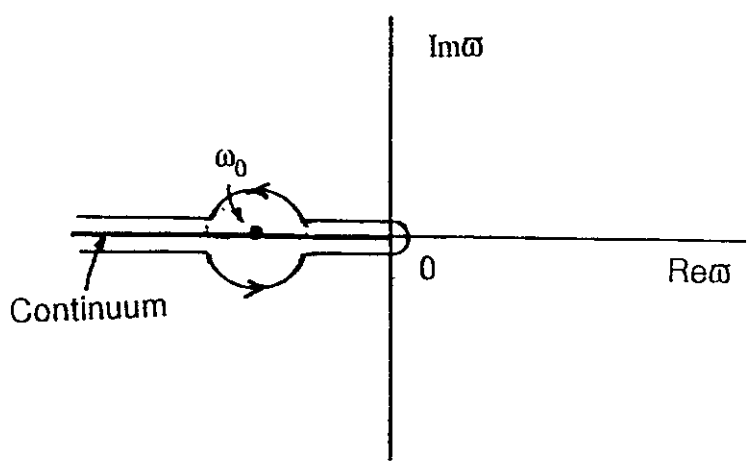
Imϖ
ω_0
0
Reϖ
Continuum

Fig.6

Recent Issues of NIFS Series

NIFS-363 A. Ida, H. Sanuki and J. Todoroki
An Extended K-dV Equation for Nonlinear Magnetosonic Wave in a Multi-Ion Plasma; June 1995

NIFS-364 H. Sugama and W. Horton
Entropy Production and Onsager Symmetry in Neoclassical Transport Processes of Toroidal Plasmas; July 1995

NIFS-365 K. Itoh, S.-I. Itoh, A. Fukuyama and M. Yagi,
On the Minimum Circulating Power of Steady State Tokamaks; July 1995

NIFS-366 K. Itoh and Sanae-I. Itoh,
The Role of Electric Field in Confinement; July 1995

NIFS-367 F. Xiao and T. Yabe,
A Rational Function Based Scheme for Solving Advection Equation; July 1995

NIFS-368 Y. Takeiri, O. Kaneko, Y. Oka, K. Tsumori, E. Asano, R. Akiyama, T. Kawamoto and T. Kuroda,
Multi-Beamlet Focusing of Intense Negative Ion Beams by Aperture Displacement Technique; Aug. 1995

NIFS-369 A. Ando, Y. Takeiri, O. Kaneko, Y. Oka, K. Tsumori, E. Asano, T. Kawamoto, R. Akiyama and T. Kuroda,
Experiments of an Intense H- Ion Beam Acceleration; Aug. 1995

NIFS-370 M. Sasao, A. Taniike, I. Nomura, M. Wada, H. Yamaoka and M. Sato,
Development of Diagnostic Beams for Alpha Particle Measurement on ITER; Aug. 1995

NIFS-371 S. Yamaguchi, J. Yamamoto and O. Motojima;
A New Cable -in conduit Conductor Magnet with Insulated Strands; Sep. 1995

NIFS-372 H. Miura,
Enstrophy Generation in a Shock-Dominated Turbulence; Sep. 1995

NIFS-373 M. Natsir, A. Sagara, K. Tsuzuki, B. Tsuchiya, Y. Hasegawa, O. Motojima,
Control of Discharge Conditions to Reduce Hydrogen Content in Low Z Films Produced with DC Glow; Sep. 1995

NIFS-374 K. Tsuzuki, M. Natsir, N. Inoue, A. Sagara, N. Noda, O. Motojima, T. Mochizuki, I. Fujita, T. Hino and T. Yamashina,
Behavior of Hydrogen Atoms in Boron Films during H_2 and He Glow Discharge and Thermal Desorption; Sep. 1995

NIFS-375 U. Stroth, M. Murakami, R.A. Dory, H. Yamada, S. Okamura, F. Sano and T. Obiki,
Energy Confinement Scaling from the International Stellarator Database; Sep. 1995

NIFS-376 S. Bazdenkov, T. Sato, K. Watanabe and The Complexity Simulation Group,
Multi-Scale Semi-Ideal Magnetohydrodynamics of a Tokamak Plasma; Sep. 1995

NIFS-377 J. Uramoto,
Extraction of Negative Pionlike Particles from a H2 or D2 Gas Discharge Plasma in Magnetic Field; Sep. 1995

NIFS-378 K. Akaishi,
Theoretical Consideration for the Outgassing Characteristics of an Unbaked Vacuum System; Oct. 1995

NIFS-379 H. Shimazu, S. Machida and M. Tanaka,
Macro-Particle Simulation of Collisionless Parallel Shocks; Oct. 1995

NIFS-380 N. Kondo and Y. Kondoh,
Eigenfunction Spectrum Analysis for Self-organization in Dissipative Solitons; Oct. 1995

NIFS-381 Y. Kondoh, M. Yoshizawa, A. Nakano and T. Yabe,
Self-organization of Two-dimensional Incompressible Viscous Flow in a Friction-free Box; Oct. 1995

NIFS-382 Y.N. Nejoh and H. Sanuki,
The Effects of the Beam and Ion Temperatures on Ion-Acoustic Waves in an Electron Beam-Plasma System; Oct. 1995

NIFS-383 K. Ichiguchi, O. Motojima, K. Yamazaki, N. Nakajima and M. Okamoto
Flexibility of LHD Configuration with Multi-Layer Helical Coils; Nov. 1995

NIFS-384 D. Biskamp, E. Schwarz and J.F. Drake,
Two-dimensional Electron Magnetohydrodynamic Turbulence; Nov. 1995

NIFS-385 H. Kitabata, T. Hayashi, T. Sato and Complexity Simulation Group,
Impulsive Nature in Collisional Driven Reconnection; Nov. 1995

NIFS-386 Y. Katoh, T. Muroga, A. Kohyama, R.E. Stoller, C. Namba and O. Motojima,
Rate Theory Modeling of Defect Evolution under Cascade Damage Conditions:The Influence of Vacancy-type Cascade Remnants and Application to the Defect Production Chracterization by Microstructural Analysis; Nov. 1995

NIFS-387 K. Araki, S. Yanase and J. Mizushima,
Symmetry Breaking by Differential Rotation and Saddle-node Bifurcation of the Thermal Convection in a Spherical Shell; Dec. 1995

NIFS-388 V.D. Pustovitov,
Control of Pfirsch-Schlüter Current by External Poloidal Magnetic Field in Conventional Stellarators: Dec. 1995

NIFS-389 K. Akaishi,
On the Outgassing Rate Versus Time Characteristics in the Pump-down of an Unbaked Vacuum System; Dec. 1995

NIFS-390 K.N. Sato, S. Murakami, N. Nakajima, K. Itoh,
Possibility of Simulation Experiments for Fast Particle Physics in Large Helical Device (LHD); Dec. 1995

NIFS-391 W.X.Wang, M. Okamoto, N. Nakajima, S. Murakami and N. Ohyabu,
A Monte Carlo Simulation Model for the Steady-State Plasma in the Scrape-off Layer; Dec. 1995

NIFS-392 Shao-ping Zhu, R. Horiuchi, T. Sato and The Complexity Simulation Group,
Self-organization Process of a Magnetohydrodynamic Plasma in the Presence of Thermal Conduction; Dec. 1995

NIFS-393 M. Ozaki, T. Sato, R. Horiuchi and the Complexity Simulation Group
Electromagnetic Instability and Anomalous Resistivity in a Magnetic Neutral Sheet; Dec. 1995

NIFS-394 K. Itoh, S.-I Itoh, M. Yagi and A. Fukuyama,
Subcritical Excitation of Plasma Turbulence; Jan. 1996

NIFS-395 H. Sugama and M. Okamoto, W. Horton and M. Wakatani,
Transport Processes and Entropy Production in Toroidal Plasmas with Gyrokinetic Eletromagnetic Turbulence; Jan. 1996

NIFS-396 T. Kato, T. Fujiwara and Y. Hanaoka,
X-ray Spectral Analysis of Yohkoh BCS Data on Sep. 6 1992 Flares - Blue Shift Component and Ion Abundances -; Feb. 1996

NIFS-397 H. Kuramoto, N. Hiraki, S. Moriyama, K. Toi, K. Sato, K. Narihara, A. Ejiri, T. Seki and JIPP T-IIU Group,
Measurement of the Poloidal Magnetic Field Profile with High Time Resolution Zeeman Polarimeter in the JIPP T-IIU Tokamak; Feb. 1996

NIFS-398 J.F. Wang, T. Amano, Y. Ogawa, N. Inoue,
Simulation of Burning Plasma Dynamics in ITER; Feb. 1996

NIFS-399 K. Itoh, S-I. Itoh, A. Fukuyama and M. Yagi,

Theory of Self-Sustained Turbulence in Confined Plasmas; Feb. 1996

NIFS-400 J. Uramoto,
A Detection Method of Negative Pionlike Particles from a H2 Gas Descharge Plasma; Feb. 1996

NIFS-401 K.Ida, J.Xu, K.N.Sato, H.Sakakita and JIPP TII-U group,
Fast Charge Exchange Spectroscopy Using a Fabry-Perot Spectrometer in the JIPP TII-U Tokamak; Feb. 1996

NIFS-402 T. Amano,
Passive Shut-Down of ITER Plasma by Be Evaporation; Feb. 1996

NIFS-403 K. Orito,
A New Variable Transformation Technique for the Nonlinear Drift Vortex; Feb. 1996

NIFS-404 T. Oike, K. Kitachi, S. Ohdachi, K. Toi, S. Sakakibara, S. Morita, T. Morisaki, H. Suzuki, S. Okamura, K. Matsuoka and CHS group;
Measurement of Magnetic Field Fluctuations near Plasma Edge with Movable Magnetic Probe Array in the CHS Heliotron/Torsatron; Mar. 1996

NIFS-405 S.K. Guharay, K. Tsumori, M. Hamabe, Y. Takeiri, O. Kaneko, T. Kuroda,
Simple Emittance Measurement of H- Beams from a Large Plasma Source; Mar. 1996

NIFS-406 M. Tanaka and D. Biskamp,
Symmetry-Breaking due to Parallel Electron Motion and Resultant Scaling in Collisionless Magnetic Reconnection; Mar. 1996

NIFS-407 K. Kitachi, T. Oike, S. Ohdachi, K. Toi, R. Akiyama, A. Ejiri, Y. Hamada, H.Kuramoto, K. Narihara, T. Seki and JIPP T-IIU Group,
Measurement of Magnetic Field Fluctuations within Last Closed Flux Surface with Movable Magnetic Probe Array in the JIPP T-IIU Tokamak; Mar. 1996

NIFS-408 K. Hirose, S. Saito and Yoshi.H. Ichikawa
Structure of Period-2 Step-1 Accelerator Island in Area Preserving Maps; Mar. 1996

NIFS-409 G.Y.Yu, M. Okamoto, H. Sanuki, T. Amano,
Effect of Plasma Inertia on Vertical Displacement Instability in Tokamaks; Mar. 1996

NIFS-410 T. Yamagishi,
Solution of Initial Value Problem of Gyro-Kinetic Equation; Mar. 1996